EPJ Web of Conferences **26**, 02017 (2012)
DOI: 10.1051/epjconf/20122602017

Potential of ultrafine grained materials as high performance penetrator materials

L.J. Park[1], H.J. Kim[1], C.S. Lee[2], and K.-T. Park[3,a]

[1] *Agency for Defense Development, PO Box 35-42, Daejeon 305-600, Korea*
[2] *Dept. of Mater. Sci. Eng., POSTECH, Pohang 790-784, Korea*
[3] *Dept. of Mater. Sci. Eng., Hanbat Nat'l Univ., Daejeon 305-719, Korea*

Abstract. The shear formability and the metal jet formability are important for the kinetic energy penetrator and the chemical energy penetrator, respectively. The shear formability of ultrafine grained (UFG) steel was examined, mainly focusing on the effects of the grain shape on the shear characteristics. For this purpose, UFG 4130 steel having the different UFG structures, the lamellar UFG and the equiaxed UFG, was prepared by equal channel angular pressing (ECAP). The lamellar UFG steel exhibited more sharper and localized shear band formation than the equiaxed UFG steel. This is because a lamellar UFG structure was unfavourable against grain rotation which is a main mechanism of the band propagation in UFG materials. Meanwhile, the metal jet formability of UFG OFHC Cu also processed by ECAP was compared to that of coarse grained (CG) one by means of dynamic tensile extrusion (DTE) tests. CG OFHC Cu exhibited the higher DTE ductility, i.e. better metal jet stability, than UFG OFHC Cu. The initial high strength and the lack of strain hardenability of UFG OFHC Cu were harmful to the metal jet formability.

1 Introduction

Ultrafine grained (UFG) materials usually exhibit higher strength due to the Hall-Petch strengthening but lower ductility due to shear localization than coarse grained (CG) counterparts at room temperature [1]. Meanwhile, some UFG materials show high strain rate superplasticity (HSRS) at high temperatures [2]. The shear localization is beneficial for the self-sharpening of the kinetic energy penetrator. HSRS is possible to operate on the metal jet formation of the metal liner in the chemical energy penetrator [3]. Accordingly, UFG materials are promising as the high performance penetrator materials. In this study, the shear localization behaviour of UFG steel was examined focusing on the effects of the grain shape. Besides, the metal jet formability of UFG Cu was compared to that of CG counterpart by means of the dynamic tensile extrusion test.

2 Experimental

4130 steel and OFHC Cu were selected as the model materials to examine the shear localization and the metal jet formability, respectively. Both were subjected to equal channel angular pressing (ECAP) in order to fabricate a UFG structure. Tempered martensitic 4130 steel was subject to 4 passes of ECAP with routes A and B_c at 400 °C. Routes A and B_c with 4 passes resulted in a lamellar UFG structure and an equiaxed UFG structure, respectively [4]. Well-annealed OFHC Cu was subjected to 16 passes of ECAP with route C at room temperature. Route C of 16 passes also introduced an equiaxed UFG structure [4].

In order to examine the shear localization behavior, tensile tests with the initial strain rate of 10^{-3} s^{-1} were carried out on both lamellar and equiaxed UFG 4130 steels. The shear localization during tensile test was monitored by a high speed camera.

Dynamic tensile extrusion (DTE) [5] was employed to examine the metal jet formability of CG and UFG OFHC Cu. DTE tests were carried out by launching the sphere sample (ϕ 7 mm) using a gas gun in vacuum toward the DTE die shown in figure 1 (the dimensions in mm) which stands apart by 5 m from the sample launching station. The sample velocity just before reaching the DTE die was ~ 500 m/sec. The metal jet fragmentation after DTE was captured by using a high speed camera installed at the exit of the DTE die.

The microstructures were examined by using electron back scatter diffraction. EBSD was obtained on the electropolished plane parallel to the DTE axis by using a Helios nanolab^{TM} 600 with the acceleration voltage of 30 kV and the scanning step size of 25 nm (a confidence index of 0.22 ~0.42).

3 Results and discussion

3.1 Shear localization of UFG 4130 steel

Figure 2 shows the microstructures of 4130 steel after ECAP. A lamellar UFG structure was well-developed by 4 passes ECAP with route A (figure 2(a)). The lamellar width was ~100 nm. In contrast, 4 passes ECAP with Route B_c resulted in an equiaxed UFG structure of the grain size of ~300 nm (figure 2(b)). The corresponding selected area diffraction pattern was in the ring configuration with diffused spots for both cases, indicating that a considerable portion of boundaries was high-angled.

Figure 3(a) shows the nominal stress–strain curves of two UFG 4130 steels; for the purpose comparison, that of the unECAPed steel was also presented. While the unECAPed steel exhibited moderate strain hardening

[a] e-mail: ktpark@hanbat.ac.kr

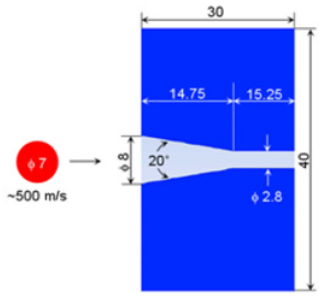

Fig. 1. The Schematic of the present DTE die.

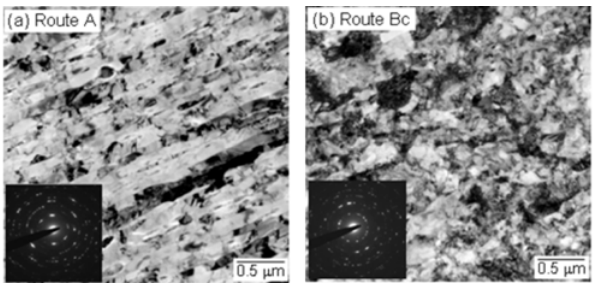

Fig. 2. TEM micrographs of 4130 steel after 4 passes ECAP with (a) route A and (b) route B_c.

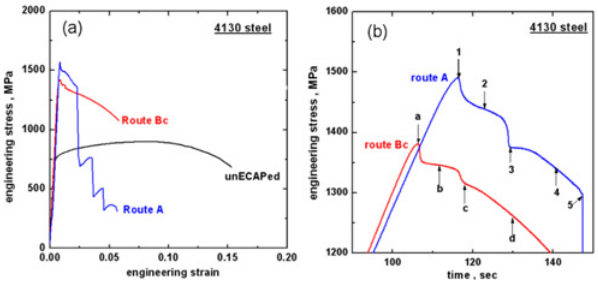

Fig. 3. (a) Nominal stress–strain curves of two UFG 4130 steels and unECAPed one, (b) the corresponding stress–time curves of two UFG 4130 steels.

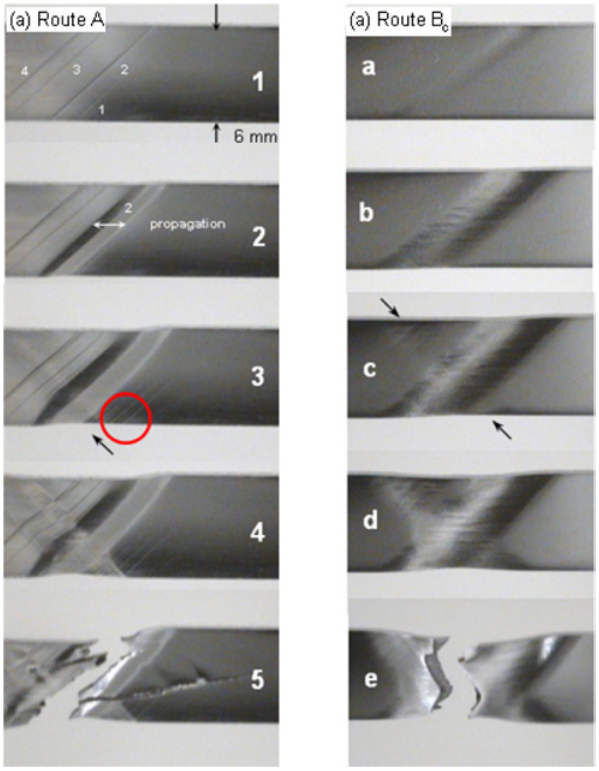

Fig. 4. The images of the gage section of (a) the lamellar and (b) equiaxed UFG 4130 steels showing the sequence of shear band formation during tensile test captured by a high speed camera.

after yielding, two UFG steels showed abrupt stress drop upon yielding, indicating the shear failure. For a close inspection, the corresponding stress–time curves of two UFG steels are constructed in figure 3(b). Both UFG steels showed two abrupt stress drops during plastic flow, each followed by strain softening.

The images of the deforming gage section of two UFG steels during tensile tests captured by using a high speed camera are shown in figure 4: the number and alphabet in Fig. 4 match with those in Fig. 3(b) indicated by the arrows. In the case of the lamellar UFG steel processed by route A (figure 4(a)), several sharp shear bands appeared upon yielding and only one band among them began to propagate along the stress axis. Then, a conjugate band showed up intersecting the first formed bands by 90°. Finally, a breakage occurred along the first-formed propagating band. In contrast, only one broad shear band with diffusive boundaries was developed upon yielding in the equiaxed UFG steel processed by route B_c (figure 4(b)). A broad conjugated band also appeared intersecting the first-formed broad band by 90° like the lamellar UFG one.

However, a breakage occurred in a zigzag pattern along both shear bands. The match between figures 3(b) and 4 revealed that the first abrupt stress drop upon yielding was caused by the first shear band formation and the second abrupt stress drop during plastic flow was attributed to the conjugate shear band formation. The strain softening after the abrupt stress drop was obviously related to the shear band propagation.

As aforementioned, shear localization is more severe in UFG materials than in CG counterparts because the lack of strain accommodation ability in the former in association with the limited dislocation activity in a UFG structure. Besides, figure 4 clearly reveals that the shear localization is affected not only by the grain size but also the grain morphology. The previous investigations explained the enhanced shear localization in UFG/nanocrystalline materials in terms of grain rotation: due to the space limit, the grain rotation models for shear localization in UFG/nanocrystalline materials are not described here, but they are well summarized in reference [6]. Most grain rotation models suggested in the literature assume the equiaxed grain structure. The equiaxed grains are favourable for grain rotation but the lamellar grains are unfavourable. Therefore, it is expected that shear localization in the lamellar UFG materials is more severe than in the equiaxed UFG materials, indicating the strong potential of the lamellar UFG materials as the high performance kinetic energy penetrator materials by enhancing the self-sharpening property.

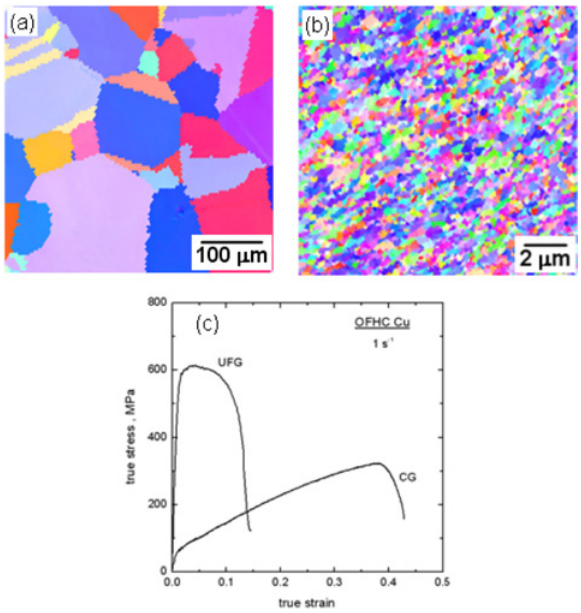

Fig. 5. (a) EBSD IPF map of CG Cu, (b) EBSD IPF map of UFG Cu, (c) true stress–strain curves of CG Cu and UFG Cu tensile-tested at 10^{-3} s^{-1}.

3.2 DTE behaviour of UFG OFHC Cu

The EBSD inverse pole figures (IPF) of well-annealed CG Cu and UFG Cu (16 passes ECAP with route B_c) before DTE are shown in figure 5. The grain size of CG Cu and UFG Cu was ~120 μm and 0.3 μm, respectively. The grains of both Cu were equiaxed and their texture was fairly random. The true stress–strain curves of CG Cu and UFG Cu are shown in figure 5(c). CG Cu exhibited the low yield strength of ~ 50 MPa and extensive strain hardening reaching the tensile strength of ~320 MPa and the total elongation of 43%. In contrast, UFG Cu showed a very brief strain hardening after yielding, i.e. near perfect plasticity. As similar to other UFG materials, its yield strength was over 10 times higher but the total elongation was much lower, compared to the CG counterpart.

The high speed camera photographs of CG and UFG OFHC Cu at the exit moment of DTE and their recovered fragments are shown in figure 6. CG Cu was fragmented into 4 pieces while UFG Cu was fragmented into 2 pieces: the unnumbered piece in the figure is the remnant remained in the DTE die. The DTE ductility of CG Cu and UFG Cu were ~570% and ~240%, respectively: the DTE ductility is the sum of the ductility of each fragment with respect to the initial sample diameter. All fragments were in the lenticular shape, indicating that fragmentation occurred by the plastic instability (i.e. necking) rather than by void coalescence.

Obviously, the CG sample exhibited much higher total DTE ductility. The above DTE behavior of CG Cu and UFG Cu indicate that CG Cu would possess the better metal jet formability than UFG Cu. The fragmentation of the metal jet, i.e. the metal jet stability, depends on the balance between the kinetic energy related to the

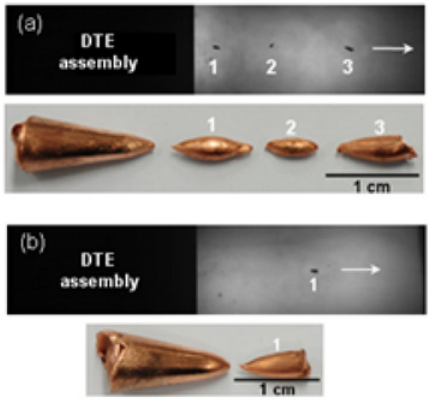

Fig. 6. The high speed photographs of (a) CG and (b) UFG OFHC Cu at the exit moment of DTE and their recovered fragments.

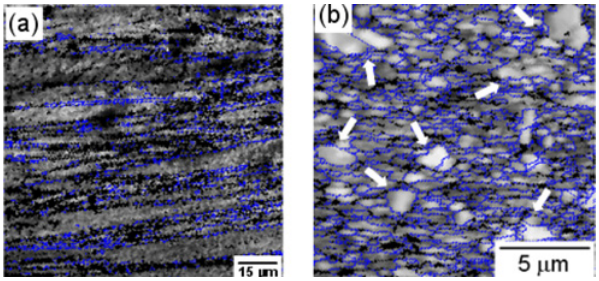

Fig. 7. EBSD image quality maps of the fragments of (a) CG Cu and (b) UFG Cu: the DTE axis is horizontal.

radial inertia force suppressing the plastic instability (i.e. the inertia term) and the plastic work dissipated during fragmentation (i.e. the plastic term) [7,8]. On the basis of the energy balance, the metal jet stability is often described by the time-dependent dimensionless parameter (Γ(t)) [8].

$$\Gamma^2(t) = 3^{1/2}\rho\varepsilon^2(t)a^2(t)/Y \qquad (1)$$

where ρ, ε(t), a(t), and Y are the density, strain rate, jet radius and yield stress at time t (equivalent to plastic flow stress). The metal jet stability decreases as Γ decreases. As the metal jet stretches, Γ decreases in conjunction with the corresponding decrease of the strain rate and the jet radius. The contribution of the flow stress to the metal jet stability depends on the mechanical state of the materials. For the strain hardening materials like the present CG OFHC Cu, the flow stress increases during the jet stretching as shown in figure 5(c). So Γ decreases and the metal jet becomes more unstable. In contrast, UFG OFHC has much higher yield and flow stresses and exhibit very brief strain hardening. The higher flow stress of UFG OFHC Cu results in the smaller Γ than CG counterpart and makes its jet unstable initially.

During dynamic deformation at high strain rates, adiabatic heating is significant and therefore dynamic recrystallization which may affect the metal jet formability is expected to occur. The EBSD image quality maps of the fragments of CG Cu and UFG Cu ('1' in figure 6) are shown in figure 7. In the case of CG Cu, initially coarse grains were severely elongated along the DTE axis without

dynamic recrystallization. In contrast, the dynamically recrystallized grains of several μm were easily found in UFG Cu, as indicated by the arrows in figure 7(b). This indicates that UFG Cu processed by multi-pass ECAP was initially in a high energy state due to severe plastic deformation. It was reported that the existence of dynamically recrystallized fine grains may be beneficial for enhancing the metal jet formability of CG Cu in relation to HSRS [3]. However, in the present case, the dynamically recrystallized grains were embedded into unrecrystallzed UFG grains which were elongated along the DTE axis. This microstructure is not expected to induce HSRS.

4 Conclusions

(1) The lamellar UFG steel exhibited the better shear formability, i.e. the more sharper and localized shear band formation, than the equiaxed UFG steel. This is due to the fact that a lamellar UFG structure suppresses grain rotation which is a main mechanism of shear band formation in UFG materials.

(2) CG OFHC Cu exhibited the better DTE ductility, a measure of the metal jet stability, than UFG OFHC Cu. The inferior metal jet stability of UFG OFHC Cu is caused by its initial higher strength and lack of strain hardenability compared to CG OFHC Cu.

Acknowledgement

This study was supported by a grant from the Basic Research Program of the Agency for Defense Development of Republic of Korea under the contract No. UD100002GD.

References

1. Q. Wei, T. Jiao, K. T. Ramesh and E. Ma, Scripta Mater. **50**, 359 (2004)
2. D. H. Shin, D. Y. Hwang, Y. J. Oh, K. -T. Park, Metall. Mater. Trans. A **35A**, 825 (2004)
3. A. H. Chokshi, M. A. Meyers, Scripta Metall. Mater. **24**, 605 (1990)
4. M. Furukawa, Z. Horita and T. G. Langdon, Mater. Sci. Eng. **A332**, 97 (2002)
5. G. T. Grey III, E. Cerreta, C. A. Yablinsky, L. B. Addessio, B. L. Henrie, B. H. Sencer, M. Burkett, P. J. Maudlin, S. A. Maloy, C. P. Trujillo, M. F. Lopez, in *Shock Compression of Condense Matter*, ed. by M. D. Furnish, M. Elert, T. P. Russell, C. T. White, Americ. Inst. of Phys. (2006) 725.
6. L. J. Park, H. W. Kim, J. D. Yoo, C. S. Lee, K. -T. Park, Mater. Sci. Eng. **A527**, 645 (2010)
7. D. E. Grady, Int. J. Impact Engng. **5**, 285 (1987)
8. L. A. Romero, J. Appl. Phys. **65**, 3006 (1989) 3006